Journal of Photonics for Energy

SPIEDigitalLibrary.org/jpe

Numerical analysis of exciton dynamics in organic light-emitting devices and solar cells

Daniele Rezzonico
Benjamin Perucco
Evelyne Knapp
Roger Häusermann
Nils A. Reinke
Felix Müller
Beat Ruhstaller

SPIE

Numerical analysis of exciton dynamics in organic light-emitting devices and solar cells

Daniele Rezzonico,[a] Benjamin Perucco,[a] Evelyne Knapp,[b] Roger Häusermann,[b] Nils A. Reinke,[b] Felix Müller,[a] and Beat Ruhstaller[a,b]

[a] Fluxim AG, Winterthur, 8835 Feusisberg, Switzerland

[b] Zurich University of Applied Sciences, Institute of Computational Physics, Winterthur, 8401 Switzerland

beat.ruhstaller@zhaw.ch

Abstract. We demonstrate the importance of a comprehensive modeling of the dynamics of excited states in organic optoelectronics devices. Our numerical analysis demonstrates that exciton distributions extracted from spectral emission measurements of OLEDs are equivalent to those obtained by solving charge and exciton transport equations when the position-dependent coupling to optical modes is taken into account. The transport simulations are based on the extended Gaussian disorder model for organic semiconductors. Further, we show that the same numerical modeling framework can be used to accurately simulate bulk-heterojunction organic solar cells with dissociation of charge-transfer excitons. The simulations are compared to experimental data. [DOI: 10.1117/1.3528045]

Keywords: OLEDs, solar cells; organic semiconductors; device simulation; parameter extraction; optimization; excitons; disorder model.

Paper 10141SSP received Aug. 15, 2010; accepted for publication Nov. 22, 2010; published online Jan. 13, 2011.

1 Introduction

Organic optoelectronic devices are exploited in various applications that range from display and the lighting in the case of organic light-emitting devices (OLEDs), to solar cells, sensors and wearable electronics. Often, the advantage of a nearly unlimited variety of materials is diminished by time-consuming and complicated experimental optimization procedures. Numerical simulations have become indispensable for gaining insight into the device physics, for extracting physical parameters that govern electrical and optical characteristics, and for optimizing device performance. We first present a comprehensive model for charge, exciton, and photon processes in OLEDs that extends a previously reported device model.[1,2] We then demonstrate the impact of the multilayer environment on the radiative excitons in OLEDs and confirm the resulting exciton distribution by solving the inverse outcoupling problem for a polymer-based OLED. Subsequently, we model the dissociation dynamics of charge-transfer (CT) excitons in bulk-heterojunction organic solar cells. For that purpose the exciton rate equation is modified and the optical part of the model considers light penetration and absorption in the solar cell structure. These models are now implemented in the commercially available software SETFOS.[3] The relevant sequence of processes is illustrated in Fig. 1. Figure 1 summarizes the optoelectronic processes in organic semiconductors implemented in SETFOS. In addition to these physical processes, SETFOS also provides algorithms for nonlinear optimization and fitting.

2 OLEDS: Device Model and Results

The external quantum efficiency of OLEDs is given as the product of charge carrier balance, exciton generation efficiency, photoluminescence quantum yield and outcoupling efficiency.

1947-7988/2011/$25.00

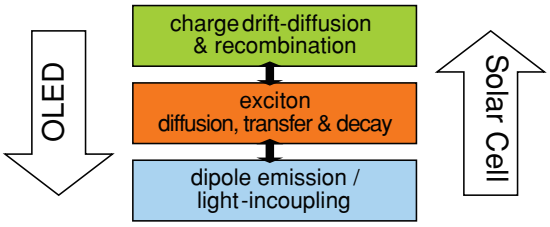

Fig. 1 Simulation workflow of SETFOS for optoelectronic device simulation of organic light-emitting and light-harvesting devices.

Excitons play a crucial role in device operation, since they are produced by electron-hole recombination in some position in the device and may travel by diffusion before decaying radiatively. The radiative decay itself, too, depends on the position, since the coupling to the optical modes is position-dependent. In the following we review the main ingredients for a full numerical description of OLED operation, starting with the charge transport model, which affects the current balance and indirectly, through the exciton transport equation, the optical outcoupling efficiency. As we show below, these processes are accessible to numerical simulations.

2.1 *Transport Model with Energetic Disorder*

For an accurate description of all physical processes contributing to the carrier balance in OLEDs and thus to the generation of the excitons, advanced models governing charge injection and transport are needed.

Due to their disordered nature, polymers and small molecules have broadened highest occupied molecular orbital (HOMO) and lowest unoccupied molecular orbital (LUMO) energy levels, as illustrated in Fig. 2(a). The charge transport in such semiconductors is therefore characterized by charge mobilities that depend on the energetic disorder of the molecular orbitals. The extended Gaussian disorder model foresees a Gaussian density of states (DOS) that accounts for such a statistical distribution of energy states. The zero-field mobility has been demonstrated to depend on the DOS broadening σ as $\mu_0(T) = \mu_0 \exp(-C\sigma^2)$ (Ref. 4) while the total carrier mobility is also field- and density-dependent.

Contrarily to inorganic crystalline materials, where charge population in parabolic bands is calculated by the Boltzmann DOS statistics, this approximation no longer applies for organic semiconductors. We thus take the Fermi-Dirac distribution for determining the charge population in the Gaussian DOS. The comparison of Gaussian versus parabolic energy bands and Fermi-Dirac versus Boltzmann statistics is given in Fig. 2(b).

Besides the mobility, the energetic disorder also influences the charge injection. At metal-organic interfaces, the charge transport level is affected by the applied field and by the image charge potential, lowering therefore the injection energy barrier.[5] This effect, already known for conventional models, is even stronger when the Gaussian energy broadening of the molecular orbitals is accounted for. In fact, the more broad the HOMO or LUMO, the easier the injection from the electrodes.

The effect of the disorder parameter on the charge injection is particularly clear for devices biased below the built-in voltage as demonstrated in Fig. 3, for two values of the disorder parameter. We have demonstrated elsewhere that despite the advanced transport model with energetic disorder, the underlying partial differential equations can be efficiently solved, see Knapp *et al.*[5]

2.2 *Optical Modes and Dipole Radiation*

The outcoupling efficiency of an OLED depends on the multilayer structure. Both photon extraction and exciton profile can be optimized by calculations based on a dipole emission

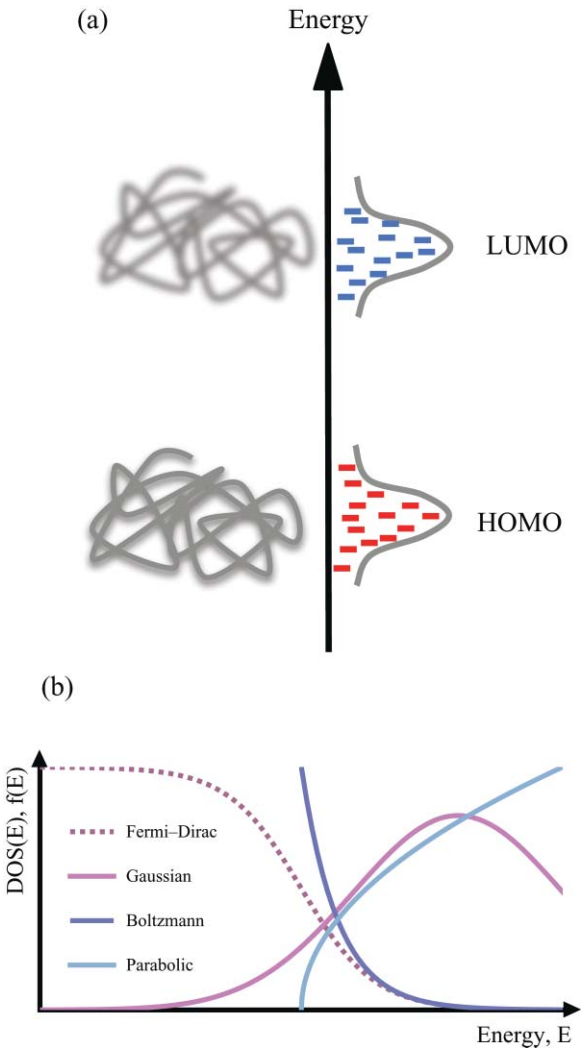

Fig. 2 (a) Gaussian broadening of the HOMO and LUMO levels in organic semiconductors. (b) The Fermi-Dirac DOS distribution may not be approximated by the Boltzmann statistics anymore.

model. On the one hand, interference effects may enhance or limit the extraction of the generated photons from the organic layers. On the other hand, radiating excitons created by recombination of charges feel the optical feedback from the multilayer system leading to a spatially resolved exciton kinetics.

We illustrate the influence of the optical environment on the radiative dipoles considering a polymer LED (PLED) structure that consists of indium tin oxide (ITO)(70 nm)/Poly(3,4-ethylenedioxythiophene) poly(styrenesulfonate)(=PEDOT)(70 nm)/Polymer(80 nm)/Ba(2 nm)/Al(100 nm) on a glass substrate. Emission occurs in the polymer layer.

We perform the analysis of the optical modes with the dipole emission model in SETFOS (Ref. 3) and find the modes shown in Fig. 4(a). In this calculation we have varied the relative dipole location within the 80-nm thin active layer. The relative position 0 corresponds to the PEDOT/polymer interface and the relative position 1 to the polymer/cathode interface. Due to interference and quenching effects, the out-coupled and guided modes are suppressed and the evanescent mode is enhanced for dipole locations near the PEDOT/polymer or the polymer/cathode interface.

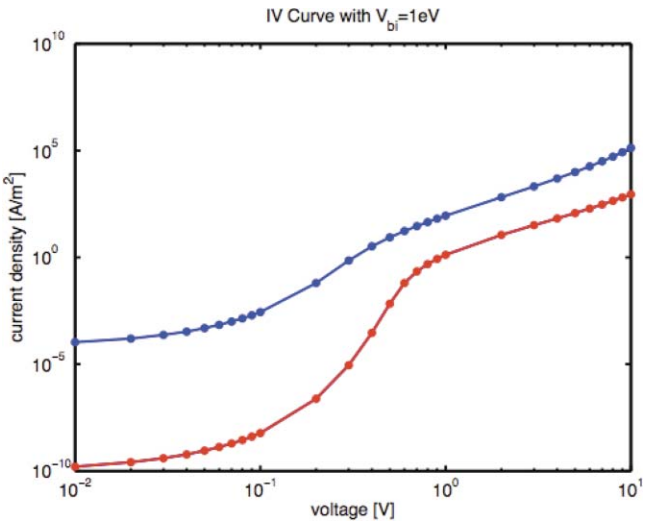

Fig. 3 Current-voltage curves for a single-layer, monopolar polymer device for disorder values of $\sigma = 0.07$ eV (red) and $\sigma = 0.14$ eV (blue). The built-in voltage is 1 V.

Correspondingly, the position dependent radiative dipole lifetime is depicted in Fig. 4(b). Note that the cavity lifetime is suppressed with respect to the free-space lifetime of 10 ns, especially near the layer interfaces.

The suppression of excited states by a reduction of their lifetime at certain positions in the device inhibits the conversion of electrical energy into outcoupled photons. Such quenching is important close to conducting layers and strongly affects the equilibrium profile of the excited states (excitons) within the emissive layers. To quantify this effect, we turn to the exciton continuity equation next.

2.3 *Exciton Dynamics*

For a comprehensive and consistent device model, the position-dependent radiative lifetime (Fig. 4) must be considered in the solution of the continuity equation for excitons species S, which then reads

$$\frac{dS(x)}{dt} = r_{\text{eff}} R(x) + \vec{\nabla} \vec{J}_s(x) - (k_r(x) + k_{nr}) S(x), \tag{1}$$

where R is the Langevin recombination term (with a user-defined pre-factor r_{eff}), and the radiative rate $k_r(x) = 1/\tau_{\text{rad}}(x)$. In Eq. (1), J_s stands for the exciton diffusion current. While the nonradiative decay rate k_{nr} is a material constant, $k_r(x)$ is now dependent on the position in the multilayer device. To illustrate the effect of the position-dependent radiative rate on the equilibrium excitons distribution, we calculated the exciton distribution for our PLED example also with the constant free-space value $k_r = 1/\tau = 0.1\ \text{ns}^{-1}$, i.e., without considering the optical feedback of the device. The result is shown in Fig. 5(a).

Without the optical feedback, the exciton density is highest at the PEDOT/polymer interface. With optical feedback, however, due to vanishing radiative lifetime (see, Fig. 4(b)) and strong evanescent coupling near the conducting PEDOT layer we also find a strongly diminished exciton density at the PEDOT/polymer interface (at $x = 140$ nm) in equilibrium. The result of Fig. 5(a) is thus consistent with the dipole calculation results in Fig. 4(b). The electronic/excitonic calculations were performed using the EGDM model for the polymer layer, for which transport parameters were assumed to be similar as those reported in Ref. 4.

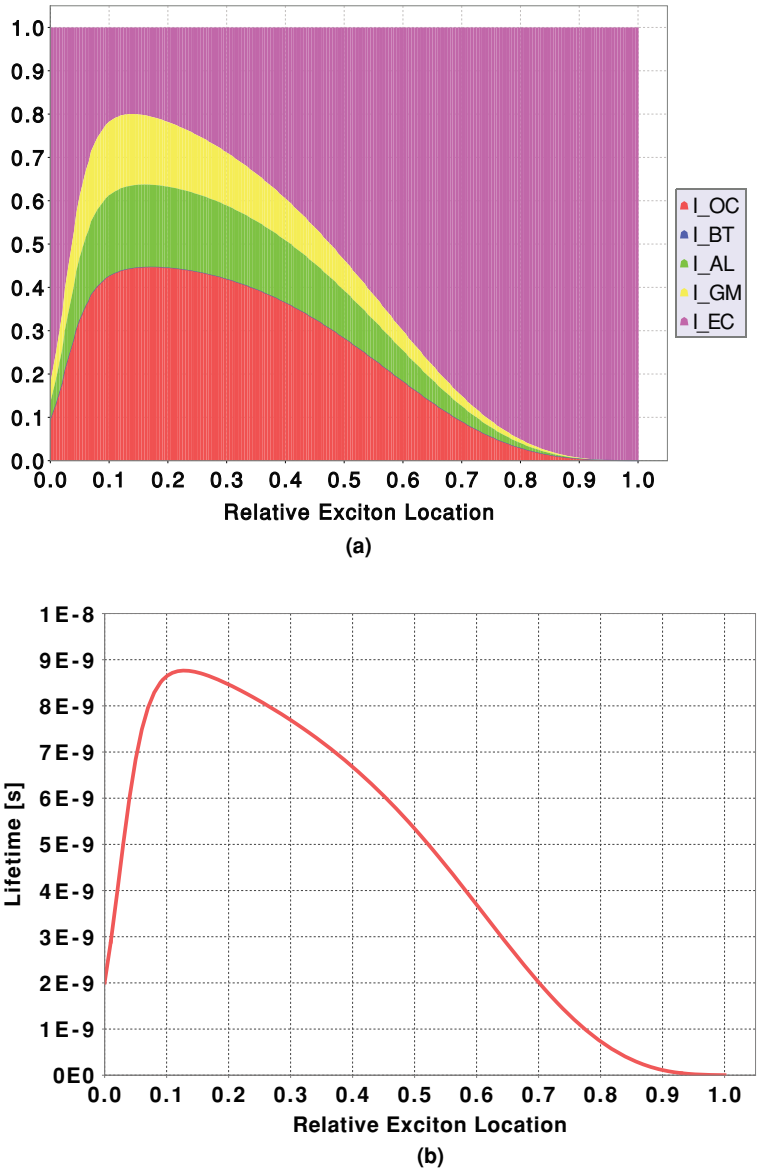

Fig. 4 (a) Analysis of light outcoupling modes of the PLED, simulated by SETFOS. The outcoupled mode (I_OC), the guided mode (I_GM), the evanescently coupled mode (I_EC), and the absorption losses (I_AL) are illustrated. (b) The calculated position-dependent radiative dipole lifetime that we use in the excitons continuity equation. The free-space lifetime is 10 ns.

2.4 *Optical Determination of the Emission Profile*

In order to illustrate the correctness of our electronic/excitonic model, that considers the optical environment, and the resulting exciton profile depicted in Fig. 5(a) we determine such profiles by an optical inverse outcoupling algorithm.[6,7] This method is implemented in SETFOS and is based on a weighting of the different emission contributions for dipoles located at various positions in the layer. The energy dissipation into evanescently coupled modes is also considered. The method is suitable for extracting a single or multiple emission zones from spectral and/or angular emission measurements.[7] We reported an extension of this method in Ref. 8, which takes an additional weighting into account based on the position-dependent dynamics of the emissive dipoles.

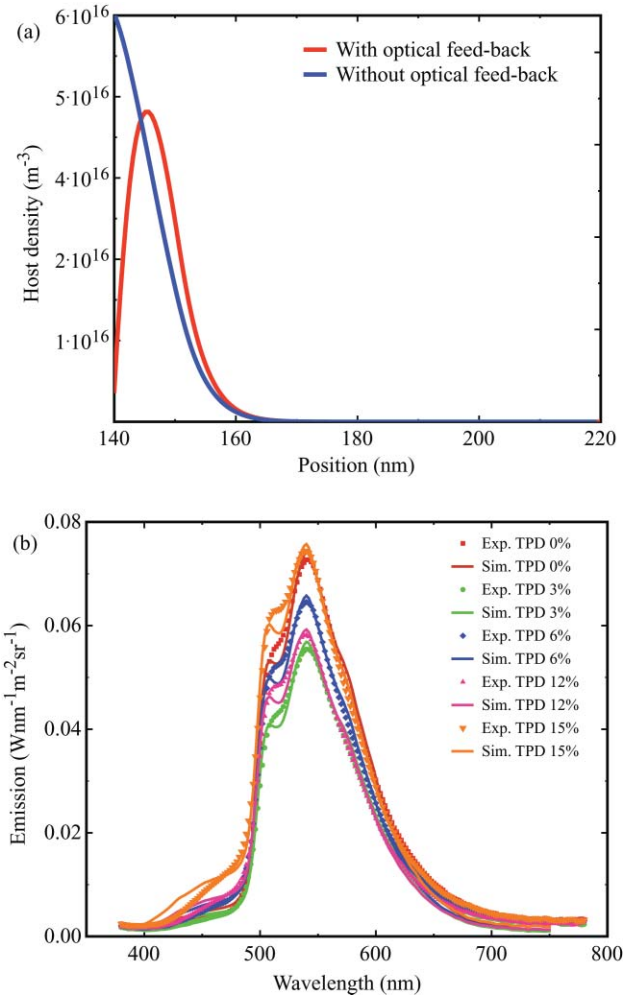

Fig. 5 (a) Calculated exciton profile with and without optical feedback. (b) Measured and fitted emission spectra for polymer blend OLEDs with PVK host emission and phosphorescent guest emission.

To illustrate this advanced inverse outcoupling algorithm with real measurement data, we examined a device similar to that described in Sec. 2.2. In this experiment, the 80-nm thin active layer is a polymer blend composed of a polyvinyl carbazole (PVK) matrix doped with electron-transport facilitating molecules of polybutadiene (PBD), hole-transport facilitating triphenyl-diamine (TPD) molecules and phosphorescent dyes. We investigated the role of the hole transport facilitating TPD molecules by varying their weight concentration. The measured emission spectra in normal direction for TPD concentrations between 0 and 15% are shown in Fig. 5(b).

The blue emission from the PVK host is diminished due to efficient energy transfer to the phosphorescent guest molecules, that emit above 500 nm. For increasing TPD concentration, the emission intensities increase as well and the spectral shapes vary slightly. The emission zones of the host excitons (in PVK) and the guest excitons are determined with the inverse outcoupling algorithm and plotted in Fig. 6.

As shown in Fig. 6(a), the PVK excitons are located close to the PEDOT/Polymer interface toward which they rapidly decay. This behavior is similar to the results found from the electronic/excitonic simulations in Fig. 5(a) and thus demonstrates that both the bottom-up electronic/excitonic simulations and the top-down optical analysis lead to very similar exciton

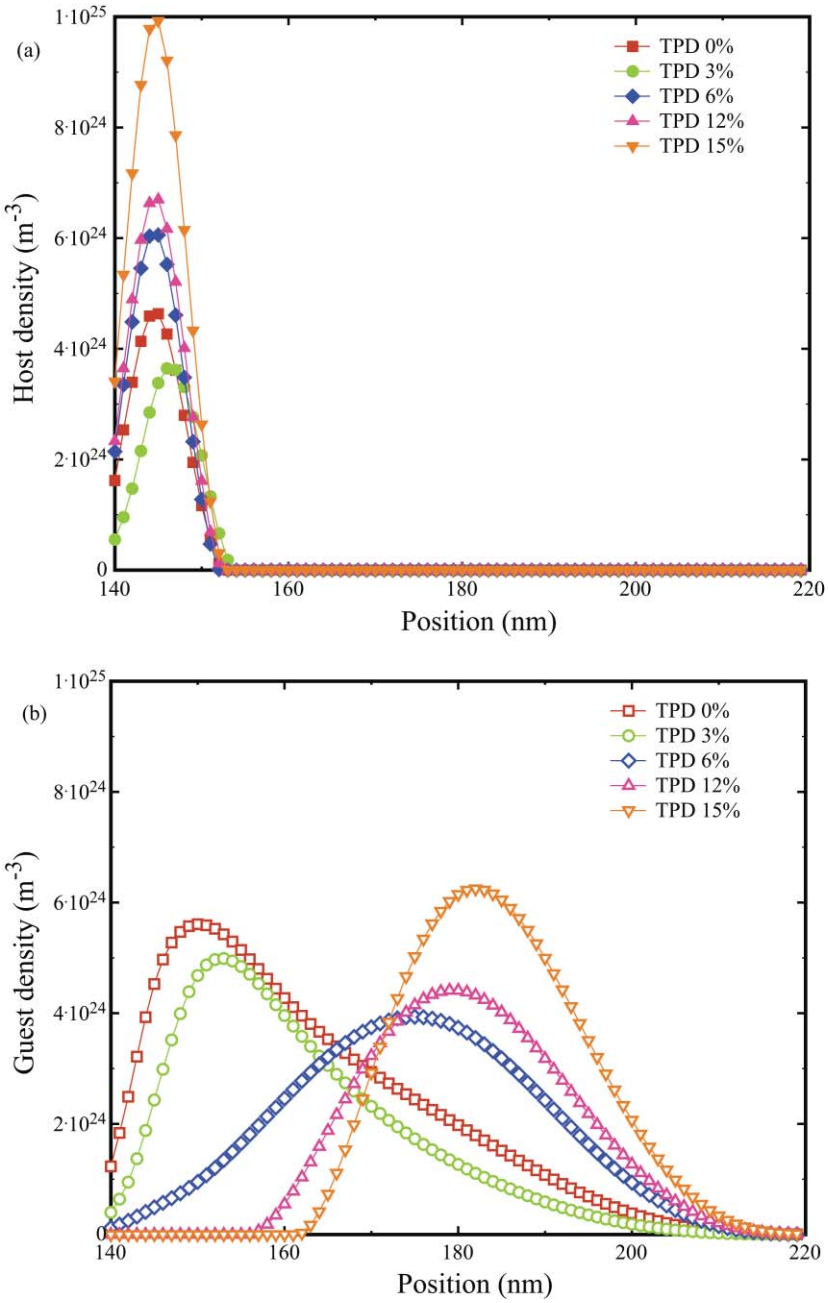

Fig. 6 (a) Host exciton density profile extracted from spectral emission measurements for varying TPD molecule weight concentration. These optically determined exciton distributions are similar to the electronically calculated ones of Fig. 5(a). (b) Guest exciton profile extracted from spectral emission measurements for varying TPD molecule weight concentration.

profiles. We have investigated this consistency further elsewhere (Perucco *et al.*[8]) with synthetic instead of experimental data.

Further, we found that the presence of the hole transporting molecule TPD shifts the emission of the phosphorescent guest molecule away from the anode and toward the center of the emissive layer, see Fig. 6(b). For small TPD concentrations, we find guest exciton distributions centered near the PEDOT interface, where they are optically quenched.

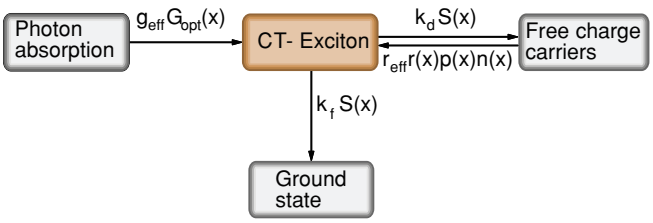

Fig. 7 Relevant processes for CT-exciton modeling.

3 Organic Solar Cells: Device Model and Results

In this second part of the paper we demonstrate the consideration of exciton dynamics for modeling organic solar cells.

3.1 *Coupling to Charge-transfer Excited States*

Often, numerical models of organic solar cells simply assume that the absorbed photon directly generates a free electron-hole pair. As a consequence, the charge drift-diffusion model has to be modified in order to suppress the electron-hole recombination into an exciton. Namely, it is common to introduce a prefactor smaller than one to the Langevin recombination term in the charge continuity equation. While this approach may be motivated by the partially inhibited bimolecular recombination in the two-phase morphology of bulk-heterojunction organic solar cells, it may not describe the field-dependent carrier generation that is often observed (see e.g., Ooi *et al.*[10]) We have ourselves recently employed the model with direct photo-generation of charges in SETFOS to successfully describe the dynamic photocurrent response of bulk-heterojunction solar cells and to analyze charge extraction by linearly increasing voltage (CELIV) formulas, see Neukom *et al.*[9] However, a physically more complete model should consider the CT exciton that is generated at the donor-acceptor interface in organic bulk-heterojunctions and which, ac-

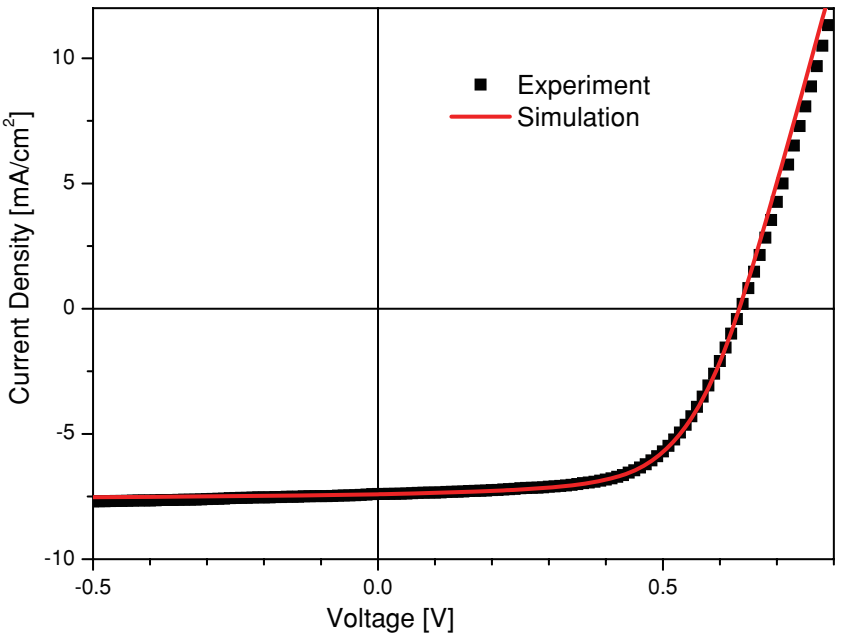

Fig. 8 Comparison of a simulated and experimentally measured current-voltage curve for an active layer thickness of 70 nm (reproduced from Ref. 11).

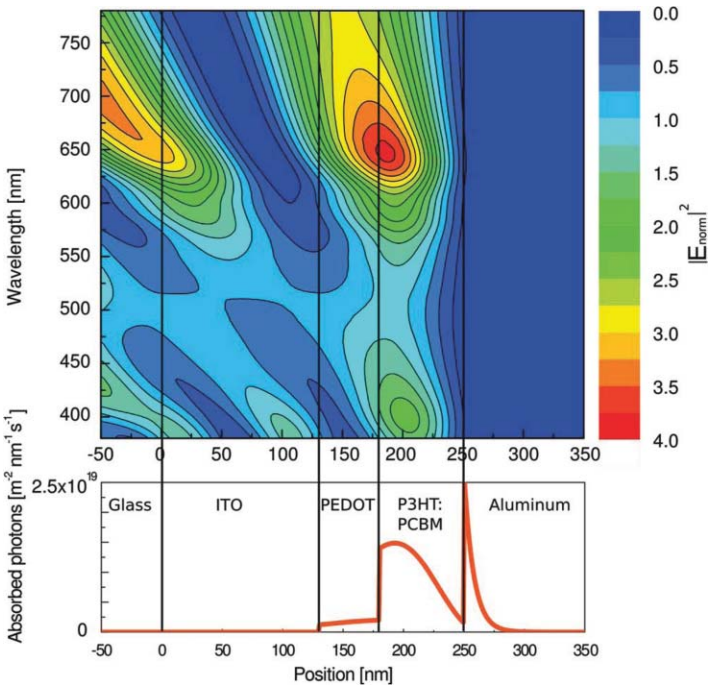

Fig. 9 Electromagnetic field penetration plot (top) is calculated using a transfer matrix formalism. This field penetration is then used to derive the photon absorption rate profile (bottom).

cording to the Onsager–Braun model,[12] may dissociate under the influence of an electric field. We have implemented this model in SETFOS and performed an analysis of the sensitivity of the steady-state and transient cell characteristics on the model parameters, see Ref. 11. CT excitons are short-lived states between the photon absorption and the generation of free charges. The excitonic processes in a bulk-heterojunction solar cell are graphically summarized in Fig. 7.

In addition to the excitonic processes present in Eq. (1), excitons are now generated from absorbed photons and can subsequently dissociate into free charges. The exciton continuity Eq. (1) is therefore modified and becomes

$$\frac{dS(x)}{dt} = r_{\text{eff}} R(x) - (k_d + k_{nr}) S(x) + g G_{\text{opt}}(x). \tag{2}$$

$G_{\text{opt}}(x)$ is the photon absorption profile calculated by transfer matrix formalism and g an user-defined prefactor. The absorbed photons generate excited states instead of free charges. The exciton dissociation term $k_d S(x)$ in Eq. (6) couples then to the charge continuity equations as a charge generation term. k_d is the exciton dissociation rate calculated by the Onsager and Brown model.[12] It depends on the initial free separation distance a, which is typically on the order of magnitude of the molecular dimensions.

Let us now discuss the impact of the CT-state exciton model on a P3HT-PCBM-based solar cell presented by Gilot *et al.*[13] The solar cell structure ITO(130 nm)/PEDOT(50 nm)/P3HT-PCBM/Al(100 nm) was deposited on glass and the thickness of the active layer P3HT-PCBM has been varied between 30 and 240 nm.[13] With the CT exciton continuity Eq. (2) the measured data are accurately reproduced by simulations with plausible assumptions like full Langevin recombination ($r_{\text{eff}} = 100\%$), initial pair separation distance $a = 1.3$ nm, and a decay rate k_{nr} of 10^5 s^{-1} (Ref. 11) [k_f in Fig. 7 corresponds to k_{nr} in Eq. (2)]. An example of a comparison to a P3HT-PCBM solar cell with an active layer thickness of 70 nm is depicted in Fig. 8. An active layer thickness of 70 nm corresponds to the optimal value as was shown by Gilot *et al.*[13] with the help of an experimental thickness variation. For this thickness, the charge generation

profile peaks within the active layer (P3HT:PCBM), as demonstrated by the optical simulation performed with SETFOS shown in Fig. 9. The charge generation profile records the amount of absorbed photons in the device and enters Eq. (2) as $G_{\mathrm{opt}}(x)$.

4 Conclusions

We have demonstrated the influence of the optical environment on the exciton dynamics within OLED structures by explicitly accounting for quenching effects in electronic/excitonic calculations (bottom-up approach). We therefore found exciton distributions that gradually decrease toward the quenching electrodes. Moreover, very similar emission zones (i.e., exciton distributions) were determined by analyzing experimental emission spectra with an inverse outcoupling algorithm (top-down approach). Both methods presented here, along with the extended Gaussian disorder model (EGDM), are crucial for a comprehensive understanding of the physical processes governing the outcoupling efficiency of OLEDs and therefore for their performance. We expect that our findings, demonstrated here with polymer-based OLEDs, will equally impact small-molecule based OLEDs.

Further, exciton dynamics are also important for describing excited states and charge generation in organic solar cells. Therefore, we have demonstrated in SETFOS a model for electric field dependent CT exciton dissociation and applied it to organic bulk-heterojunction solar cells.

Our numerical device model that covers all relevant processes among photons, excitons and charges provides a powerful framework for extracting material and device parameters by a combined experimental and simulation approach.

Acknowledgments

We wish to thank Michael Kiy and his colleagues from CSEM Basel for the fabrication and measurements of the polymer OLEDs investigated here (Ref. 6). Further, we thank Jan Gilot and René A. J. Janssen from TU Eindhoven for supplying us the experimental dataset of the bulk-heterojunction organic solar cells (Ref. 13). We acknowledge financial support from the European Community's Seventh Framework program under Grant agreement No. 213708 (project AEVIOM.eu) and Swiss Federal Office of Energy for supporting the POLYMOL project.

References

1. B. Ruhstaller, S. A. Carter, S. Barth, H. Riel, W. Riess, and J. C. Scott, "Transient and steady-state behavior of space charges in multilayer organic light-emitting diodes," *J. Appl. Phys.* **89**, 4575–4586 (2001).
2. B. Ruhstaller, T. A. Beierlein, H. Riel, S. Karg, J. C. Scott, and W. Riess, "Simulating electronic and optical processes in multilayer organic light-emitting devices," *IEEE J. Sel. Top. Quantum Electron.* **9**(3), 723–732 (2003).
3. Semiconducting Thin Film Optics Simulator (SETFOS) by Fluxim AG, Switzerland, www.fluxim.com.
4. S. L. M.van Mensfoort and R. Coehoorn, "Effect of Gaussian disorder on the voltage dependence of the current density in sandwich-type devices based on organic semiconductors," *Phys. Rev. B* **78**, 085207 (2008).
5. E. Knapp, R. Häusermann, H. U. Schwarzenbach, and B. Ruhstaller, "Numerical simulation of charge transport in disordered organic semiconductor devices," *J. Appl. Phys.* **108**, 054504 (2010).
6. B. Ruhstaller, T. Flatz, M. Moos, G. Sartoris, M. Kiy, T. Beierlein, R. Kern, C. Winnewisser, R. Petrot, "Optoelectronic OLED modeling for device optimization and analysis," *SID Int. Symp. Digest Tech.* Papers **38**, 1686 (2007).

7. B. Perucco, N. A. Reinke, D. Rezzonico, M. Moos, and B. Ruhstaller, "Analysis of the emission profile in organic light-emitting devices," *Opt. Express* **18**(S2), A246–A260 (2010).
8. B. Perucco, N. A. Reinke, F. Müller, D. Rezzonico, and B. Ruhstaller, "The influence of the optical environment on the emission profile and methods of its determination," *Proc. SPIE* **7722**, 14 (2010).
9. M. Neukom, N. A.Reinke, K. A.Brossi, and B. Ruhstaller, "Transient photocurrent response of organic bulk heterojunction solar cells," *Proc. SPIE* **7722**, 30 (2010).
10. Z. E. Ooi, T. L. Tam, A. Sellinger, and J. C. deMello, "Field-dependent carrier generation in bulk heterojunction solar cells," *Energy Environ. Sci.* **1**, 300–309 (2008).
11. R. Häusermann, E. Knapp, M. Moos, N. A. Reinke, Th. Flatz, and B. Ruhstaller, "Coupled optoelectronic simulation of organic bulk-heterojunction solar cells: parameter extraction and sensitivity analysis," *J. Appl. Phys.* **106**, 10450 (2009).
12. C. L. Braun, "Electric field assisted dissociation of charge transfer states as a mechanism of photocarrier production," *J. Chem. Phys.* **80**, 4157 (1984).
13. J. Gilot, I. Barbu, M. M.Wienk, and R. A. J. Janssen, "The use of ZnO as optical spacer in polymer solar cells: theoretical and experimental study," *Appl. Phys. Lett.* **91**, 113520 (2007).

Biographies and photographs of the authors not available.